REDUCED SENSOR BASED PMSM DRIVEN AUTONOMOUS SOLAR WATER PUMPING SYSTEM

[1]HOUJI HEMANTH SAGAR

PG scholar, Department of Electrical and Electronics Engineering, Vidya Jyothi Institute of Technology Vjit, Hyderabad, India.

[2]V.VIJAYA LAKSHMI

Associate Professor, Department of Electrical and Electronics Engineering, Vidya Jyothi Institute of Technology Vjit, Hyderabad, India.

ABSTRACT

To get the most power out of a solar photovoltaic (PV) array, one must employ the maximum power point tracking (MPPT) approach due to the nonlinear v-i characteristic of solar cells. One voltage sensor and one current sensor are needed for conventional MPPT approaches. This study suggests a brand-new single sensor based maximum power point tracking (MPPT) method for pumping water from a PV array utilizing a permanent magnet synchronous motor (PMSM) drive. Since using encoders for submersible water pumping is not recommended, this study employs sensor less speed and position estimates to regulate PMSM speed. By estimating stator flux from voltages and currents in a stationary reference frame, rotor position and speed may be estimated. This paper suggests a mix multi-resonant structure for flux estimation because the traditional flux estimators have issues with saturation, DC drift, and distortion. The solar water pumping (SWP) system's cost is reduced and its dependability is increased using a sensor less speed control. The PV array's electricity is utilized to power the PMSM, which turns the pump that is connected to it. The suitability of the suggested system is illustrated using a lab-developed prototype and a digital signal processor (dSPACE-1202) to control the SWP system under various insolation circumstances.

INDEX TERMS— Frequency Locked Loop, Generalized Integrator, Maximum Power Point Tracking, and Solar Water Pumping

1. INTRODUCTION

Energy is becoming more and more necessary every day. There are not enough convectional energy sources (CESs) to meet the world's growing energy needs. Finding additional dependable energy sources is now essential in order to prevent impeding the current growth process. Solar energy is one of the numerous alternative energy sources that is receiving more attention these days. Solar energy may be used in a variety of ways. However, the popularity of solar photo-voltaic (PV) producing systems has significantly expanded due to their clean nature, noiseless operation, universal availability, long life, and reducing cost [1]. One potential use for a stand-alone solar PV producing system is solar water pumping, or SWP. For locations without connection to the utility grid and with high solar insolation, it is pretty favorable. In addition to meeting the basic human need for water, it stimulates industrial and agricultural growth in isolated regions [2].

The easiest method of running an SWP system is to connect the electric motor right to the PV array's terminals. However, because of the nonlinear v-i characteristic of solar cells, it results in an inefficient use

of PV array with a significant amount of potential solar power being wasted. A directly linked system has a utilization efficiency of 63% and 51%, respectively, for slow and rapid variable insolation, according to an experimental study conducted by Elgendy et al. [3]. Therefore, maximum power point tracking (MPPT) approaches are required to maximize the usage efficiency of PV integrated systems. The literature now in publication already has a wide variety of MPPT methods [4-5]. The two most popular MPPT methods among all are incremental conductance (INC) and perturb and observe (P&O) [6]. While the INC technique shifts the operating point where incremental conductance and instantaneous conductance are equal, the P&O algorithm operates on the principle of perturbing PV array voltage towards the maximum power point (MPP). As a result, the INC technique is more complex and computationally exhaustive than the P&O technique. Since P&O [7-9] and INC [10–12] MPPT algorithms are used by the majority of solar water pumping systems (WPS), one voltage and one current sensor are needed. However, existing sensor can be removed to reduce the cost and complexity [6], [13-21]. In order to maximize the output voltage, a flyback converter duty ratio regulation scheme is proposed in [13]. However, an envelope detection is necessary to determine the amplitude of the output voltage because it is a pulse width modulated AC. As a result, the system becomes more complicated. Furthermore, the pump in the system is driven by a 1-φ induction motor. When utilizing the same MPPT approach with a 3-φ motor, at least two output voltage sensors are needed for efficient MPPT, which results in a substantial increase in cost and complexity. The empirical relationship of a DC-DC converter has been used by several writers for single sensor MPPT. The following is the empirical relationship at MPP between voltage (Vpv), power (Ppv), and duty ratio (Dmpp):

$$\frac{\Delta V_{pv}}{\Delta D_{mpp}} = \frac{\Delta P_{pv}}{\Delta D_{mpp}} = 0 \quad (1)$$

The MPPT condition indicated in (1) has been employed by the writers in [6], [14–17]. In [6], [16], and [17], a variable step size technique is described for quick transient response. On the other hand, a variable step size approach presents a larger computing overhead and calls for system dependent constants. [18] presents a single sensor MPPT based on PV array current estimate. The PV array voltage divided by the converter resistance yields the predicted current and the equivalent resistance of the converter. Despite the fact that the aforementioned approaches, which are demonstrated to be effective in [6], [14–18], need a certain kind of DC–DC converter in order to carry out the recommended methodology. In [19], an MPPT technique is provided for a PV array that feeds the grid through a cascade H-bride multilevel inverter, detecting just grid voltage and current. However, any modification in parameters brought on by aging or temperature changes will result in an ineffective MPPT since the approach infers the MPP rather than measuring it explicitly. A capacitive load is connected to the PV array's terminals in [20]. Instantaneous power is computed and the capacitor's voltage is monitored. The MPP is tracked using the instantaneous power derivative. The instantaneous power derivative may be expressed as a second order derivative of the voltage squared of the capacitor. Despite providing a superior MPPT, this method's implementation necessitates a large computational load, slow DSP speed, and more memory requirements.

In [21], a comparatively easier MPPT technique based on tracking the charging

and discharging of a capacitor is provided. Nevertheless, steady state oscillation around MPP results from this MPPT technique. This paper presents a novel MPPT approach that just requires a voltage sensor for operation in order to address the aforementioned problems. The suggested approach depends on power estimate rather than measuring voltage and current simultaneously to calculate power. An energy-efficient motor is needed for the SWP system in order to increase efficiency and decrease the size of the PV array. For SWP, a variety of electric drives have been employed in the past, including an induction motor [2],[7], brushed DC motor [3],[8],[10], switching reluctance motor [9], and permanent magnet brushless DC motor [11]. However, permanent magnet synchronous motor (PMSM) drives are becoming more and more popular these days because of their inherent benefits, which include high efficiency, high power to weight ratio, high torque to inertia ratio, quick acceleration and deceleration capability, high power factor, high air gap flux density, and compact design [12]. An encoder assembly is needed for rotor position and speed detection in these electric motors. Usually, the rotor shaft is connected to the encoder assembly. For the reasons listed below, however, their usage is not advised for SWP [22–23]. Encoders may be expensive, and their cost varies according to

- Therefore, their price may be more in line with the motor's purchase price. Long wires are used when the WPS is installed far away.

- Are employed Long cables are used, which distorts the sensor signal and renders it inappropriate for SWP. Typically, submersible pumps are submerged in water and

- Consequently, the system dependability is decreased when mechanical sensors are used in such a hostile environment. The SWP system shuts down when the encoder fails.

- Given that the encoders are fixed to the rotor shaft, any change in

- Reprogramming the control is necessary to adjust the encoder in relation to the rotor position.

Because of the aforementioned issues with encoders, there should be significant consideration given to their usage in SWP, particularly in submersible water pumping, and a replacement solution for these sensors has to be developed. A few of the current studies provide techniques for rotor speed and position estimation based on sliding mode observers, model reference adaptive control, Kalman filters (KF), extended KF, signal injection, and reverse electro-magneto-motive force.
Nevertheless, the implementation of these techniques would need a high-end CPU due to their extensive computing demands [24]. The determination of the rotor speed and location from the stator flux offers a less computationally demanding method. However, the pure integrator used by traditional flux estimators causes saturation because of DC drift in the sensors and analog to digital converters, DC offset because of the integration's initial conditions, and distortion in the estimated flux because of low-speed harmonics in the voltage and current [25]. As a result, it is often advised to utilize a low pass filter (LPF) instead of pure integral. The choice of a single cut off frequency for the whole operating range attenuates the flux's amplitude and creates phase shift, even if the flux can be easily approximated using LPF [26]. A traditional second order generalized integrator (SOGI) based flux observer is provided in [27] to address the aforementioned issues. Nevertheless, there are two main problems with the SOGI-based estimator. These are as follows. DC offset rejection that is poor

- Subpar attenuation of lower harmonics

• In order to address the significant and unavoidable DC offset caused by offset in sensors and analog to digital converters, an enhanced SOGI (ISOGI) is proposed in [27]. Nonetheless, the noticeable lower order harmonics are still present at low speeds and in situations with uneven voltage. A multi-layer system with several levels tuned to the dominant lower harmonic is needed to lessen this issue.

For stator flux estimation, a mixed multi-resonant generalized integrator (MMGI) is therefore proposed in this study. The following are some of the planned SWP system's noteworthy contributions. Creation of an MPPT approach based on a single sensor for collecting the PV array's peak power Creation of a stator flux estimator based on MMGI for rotor position and speed estimate. With fewer sensors, the suggested PMSM-driven SWP system is created and experimentally verified with a digital signal processor (DS-12022).

2. Proposed System Configuration

The setup for the given SWP system is shown in Fig. 1. The suggested SWP system is made up of a solar PV array, a 3-φ voltage source inverter (VSI), a pump, and a PMSM, in that order. To prevent any reverse current flow between the PV array and VSI, a diode (D) is included. The suggested SWP system uses a single stage topology for SWP as Wu et al. [28] have already demonstrated that this avoids the requirement for an intermediate stage converter and is thus preferable in terms of efficiency, size, and cost. In accordance with the PV array's needed voltage and current rating, the proper number of PV modules are connected in series and parallel, respectively. Electrical energy is produced when sunlight's photons hit the PV array's surface. The VSI processes this energy and uses it to turn the motor. A pump and PMSM are mechanically connected. The pump is rotated by the PMSM, achieving the final objective of pumping water.

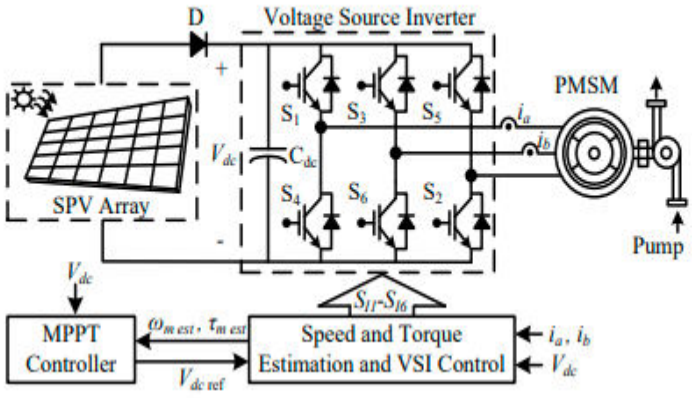

Fig. 1 System configuration diagram.

3. Proposed System Control

There are three components to the planned SWP system's control. Effective stator flux estimate utilizing an MMGI-based control method is covered in the first section. The second section addresses MPPT control, while the third section focuses on pump speed control. In the subsections that follow, the suggested control technique is thoroughly discussed.

3.1 Estimation of Stator Flux

Stator voltages and currents are used to estimate stator flux in a stationary reference frame. With the help of the switching signals (SI1, SI3, and SI5) for VSI and the observed DC link voltage (Vdc), the stator voltages in the stationary reference frame are computed. The predicted values of the stationary voltages vα and vβ are,

$$v_\alpha = \frac{V_{dc}}{3} * \left(2S_{I1} - S_{I3} - S_{I5}\right), v_\beta = \frac{V_{dc}}{3} * \left[\sqrt{3}\left(S_{I3} - S_{I5}\right)\right]$$

Based on detected stator currents (ia and ib), the stationary stator currents iα and iβ are approximated and may be written as,

$$i_\alpha = i_a,\ \ i_\beta = \frac{1}{\sqrt{3}}\left(i_a + 2i_b\right)$$

The rear emf of a PMSM is written as

$$e_{s\alpha} = v_\alpha - R_s * i_\alpha,\ \ e_{s\beta} = v_\beta - R_s * i_\beta$$

The generalized integrator (GI) based structure is used to accomplish the estimate of stator flux components. Fig. 2 shows a flux estimate based on SOGI, and the associated transfer functions (TFs) are as follows:

$$T_{\psi SOGI} = \frac{\psi_{\alpha,\beta}(s)}{e_{\alpha,\beta}(s)} = \frac{k\omega_{eest}}{s^2 + k\omega_{eest}s + \omega_{eest}^2}$$

$$T_{DSOGI} = \frac{e_{\alpha',\beta'}(s)}{e_{\alpha,\beta}(s)} = \frac{k\omega_{eest}s}{s^2 + k\omega_{eest}s + \omega_{eest}^2}$$

Where k = 2ζ, where ζ is the damping factor, and ω_{eest} is the electrical frequency in rad/s. The settling time, ts, is expressed as follows and depends on ζ:

$$t_s = \frac{4}{\zeta\omega'}$$

Since ζ ranges from 0 to 1, its value is assumed to be 0.7. As has already been mentioned in the literature, Fig. 3 illustrates that SOGI provides a subpar DC offset rejection.

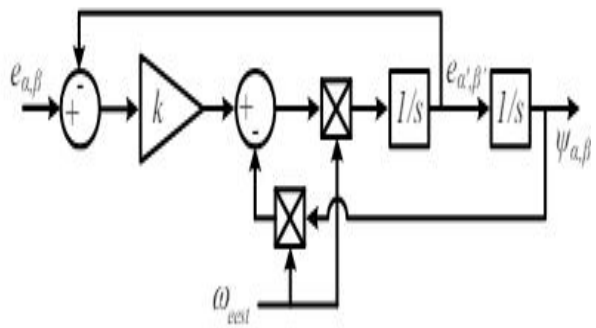

Fig. 2 SOGI based flux estimator

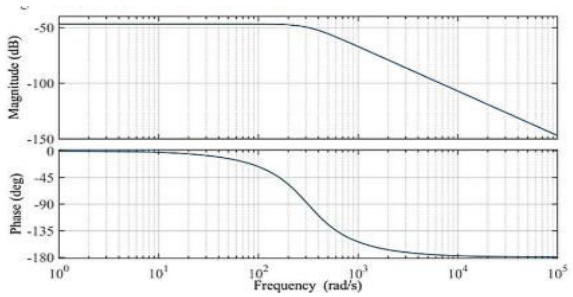

Fig. 3 Frequency response of SOGI based flux estimator

Utilizing an enhanced SOGI (ISOGI) based structure, the DC offset problem is lessened. Fig. 4 depicts the construction of the ISOGI-based flux estimator, which uses an additional loop for DC offset rejection. The following TFs are linked to it:

$$T_{\psi ISOGI} = \frac{\psi_{\alpha,\beta}(s)}{e_{\alpha,\beta}(s)} = \frac{k\omega_{eest}s}{s^3 + (k + k_{DC})\omega_{eest}s^2 + \omega_{eest}^2 s + k_{DC}\omega_{eest}^3}$$

$$T_{DISOGI} = \frac{e_{\alpha',\beta'}(s)}{e_{\alpha,\beta}(s)} = \frac{k\omega_{eest}s^2}{s^3 + (k + k_{DC})\omega_{eest}s^2 + \omega_{eest}^2 s + k_{DC}\omega_{eest}^3}$$

Fig. 5 displays the frequency response for an ISOGI-based control mechanism. The figure makes it clear that the ISOGI-based construction offers superior resistance to DC offset. It is unable to lessen the lower order harmonics, though.

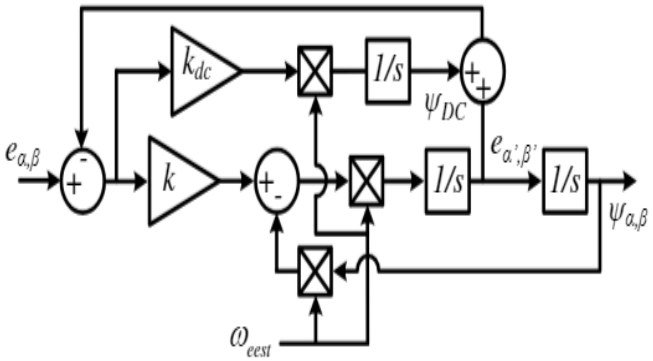

Fig. 4 ISOGI based flux estimator

This study offers a mixed multi-resonant generalized integrator (MMGI) to overcome both the difficulties, namely DC offset and dominating lower order harmonics associated with standard GI based flux estimator. The suggested structure, which consists of many GI layers—the top layer being ISOGI and the

remaining levels being SOGI—is seen in Fig. 6. The other layers help with the selective harmonic removal by resonating the matching frequency component, while the first layer functions as a band pass filter with DC offset rejection capacity. The flux estimate based on MMGI has the following TF: (10) and (11). Fig. 7 displays the frequency response for the MMGI-based control mechanism. The graphic makes it clear that the MMGI-based construction offers superior resistance to DC offset and

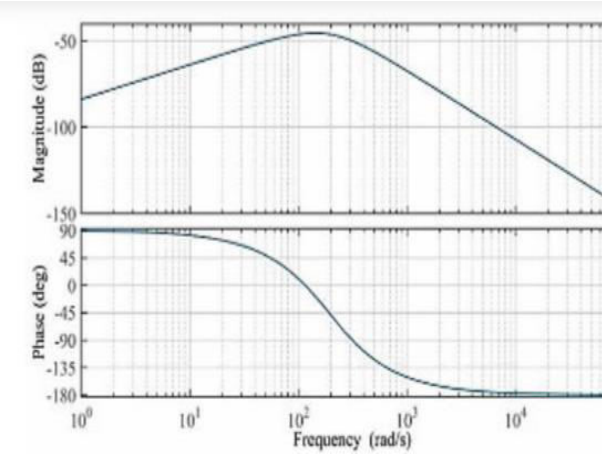

Fig. 5 Frequency response of ISOGI based flux estimator

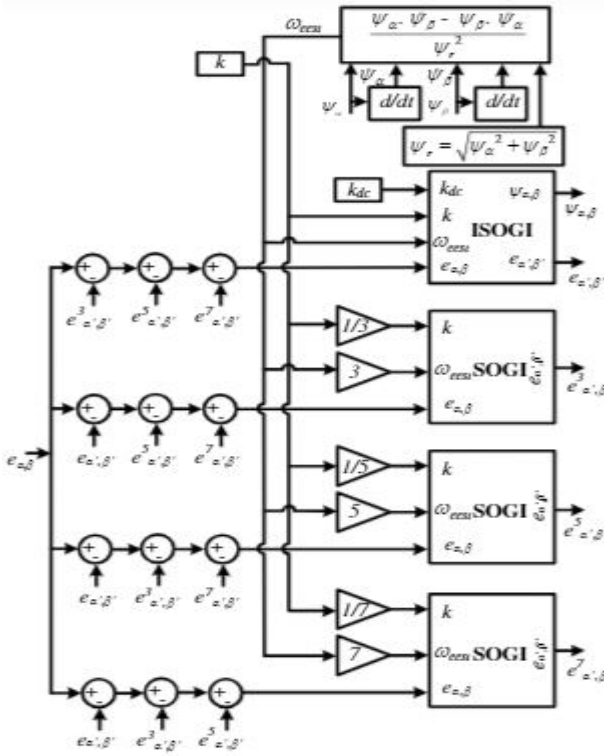

Fig. 6 MMGI based flux estimator.

Dominant harmonics of lower order. It is evident from Fig. 7 that the suggested structure attenuates the 3rd, 5th, and 7th harmonics efficiently.

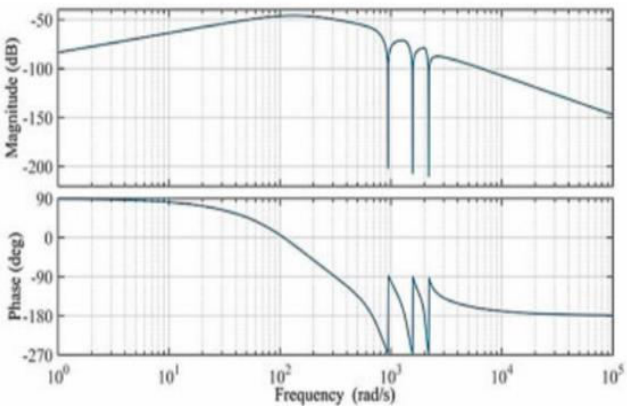

Fig. 7 Frequency response of MMGI based flux estimator

Following the estimation of the stator fluxes (ψα and ψβ) with equations (10) and (11), the resulting flux linkage (ψr) is represented as follows:

$$\psi_r = \sqrt{\psi_\alpha{}^2 + \psi_\beta{}^2}$$

3.2 Single Sensor Based MPPT

A single sensor-based MPPT approach is proposed in this paper. Two sensors are needed for traditional MPPT methods. One is a voltage sensor, which measures the voltage of the PV array, and the other is a current sensor, which measures the current of the solar PV array. The suggested method does away with the requirement for a current sensor. The following are the key components of the suggested MPPT method. The suggested MPPT system works with both single and two stage topologies and is converter independent. The cost of the system is decreased by getting rid of the PV array current sensor. The suggested system guesses the torque and speed instead of measuring them. This lowers the system cost even further. The same predicted speed that is used for MPPT is also used for speed control. This

strengthens the suggested system's resilience and dependability.

Since it is well known that the traditional P&O method affects the DC link voltage in relation to the PV power, the PV power is determined using two sensors. In this study, the estimated electromagnetic power is used instead of the PV power, and the PV voltage is adjusted to maximize the estimated electromagnetic power. Electromagnetic torque and rotor speed are the other two approximated characteristics that are used to determine electromagnetic power. The predicted stator flux and stator current components are used to calculate the electromagnetic torque (Teest), which is written as

$$T_{eest} = 3/2 * p(\psi_\alpha i_\beta - \psi_\beta i_\alpha)$$

The rotor potion estimate (θest) is provided as,

$$T_{\psi MMGI} = \frac{\psi_{\alpha,\beta}(s)}{e_{\alpha,\beta}(s)} = \left[T_{\psi ISOGI} \left(\frac{1-T_{\psi SOGI3}}{1-T_{\psi SOGI3}(s)T_{\psi ISOGI}} \right) \left(\frac{1-T_{\psi SOGI5}}{1-T_{\psi SOGI5}T_{\psi ISOGI}} \right) \left(\frac{1-T_{\psi SOGI7}}{1-T_{\psi SOGI7}T_{\psi ISOGI}} \right) \right]$$

$$T_{DMMGI} = \frac{e_{\alpha',\beta'}(s)}{e_{\alpha,\beta}(s)} = \left[T_{DISOGI} \left(\frac{1-T_{DSOGI3}}{1-T_{DSOGI3}(s)T_{DISOGI}} \right) \left(\frac{1-T_{DSOGI5}}{1-T_{DSOGI5}T_{DISOGI}} \right) \left(\frac{1-T_{DSOGI7}}{1-T_{DSOGI7}T_{DISOGI}} \right) \right]$$

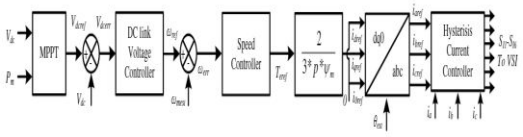

Fig. 8 Speed control of PMSM

$$\theta_{est} = \tan^{-1}\left[\frac{\psi_\beta}{\psi_\alpha} \right]$$

The estimated speed (ωmest) is given as,

$$\omega_{mest} = \frac{1}{p}\frac{d}{dt}(\theta_{est}) = \frac{\psi_\alpha . \dot{\psi}_\beta - \psi_\beta . \dot{\psi}_\alpha}{p\psi_r^2}$$

Where p is the number of pole pairs and are their respective derivatives.

Based on the predicted torque and speed, the electromagnetic power (Peest) is computed and represented as,

$$p_{eest} \quad Teest * \omega_{mest}$$

Where ωmest denotes the PMSM's estimated mechanical speed.

Following the estimation of electromagnetic power, the traditional P&O method previously described in [7-8] is adjusted for single sensor based MPPT by optimizing the estimated electromagnetic power in relation to the DC link voltage.

The suggested MPPT outputs Vdcref for a single stage structure. Vdcref generation is achieved as,

$$V_{dcref}(k) = V_{dcref}(k-1) + \delta V;\ if \begin{Bmatrix} dP_{eest} > 0 \text{ and } dV_{dc} > 0 \\ dP_{eest} < 0 \text{ and } dV_{dc} < 0 \end{Bmatrix} \quad (17)$$

$$V_{dcref}(k) = V_{dcref}(k-1) - \delta V;\ if \begin{Bmatrix} dP_{eest} > 0 \text{ and } dV_{dc} < 0 \\ dP_{eest} < 0 \text{ and } dV_{dc} > 0 \end{Bmatrix} \quad (18)$$

In this case, the difference in the DC link voltage at the kth and (k-1)th sampling instants is denoted by dVdc, while the difference in the motor output power is represented by dPeest. As previously indicated, the suggested MPPT can also operate with a two-stage WPS architecture by varying the intermediate stage converter's duty ratio (D) in the direction of maximum power. For a two-stage topology, the equations controlling MPPT operation are written as,

$$D(k) = D(k-1) - \delta d;\ if \begin{Bmatrix} dP_{eest} > 0 \text{ and } dV_{pv} > 0 \\ dP_{eest} < 0 \text{ and } dV_{pv} < 0 \end{Bmatrix}$$

$$D(k) = D(k-1) + \delta d;\ if \begin{Bmatrix} dP_{eest} > 0 \text{ and } dV_{pv} < 0 \\ dP_{eest} < 0 \text{ and } dV_{pv} > 0 \end{Bmatrix}$$

The electromagnetic power used by the presented MPPT technique is computed using motor speed and torque to produce Vdc*. Every time Vdc* is disturbed, the motor finds a new steady state speed and torque value. The motor needs greater settling time to reach the steady state value since torque and speed are mechanical variables and electromechanical systems have a much bigger mechanical time constant (Γm) than electrical time constant. Thus, in order for the MPPT technique to operate steadily, the sample period (ts) of the MPPT algorithm needs to be longer than the settling time.

3.3 Speed Control of PMSM

Fig. 8 shows the many processes in the PMSM speed control process. The reference DC link voltage (Vdcref) needed to maximize the PV array's output power is provided by the MPPT controller. When the measured DC link voltage (Vdc) and this reference voltage are compared, the voltage error (Vdcerr) is produced as,

$V_{dcerr}(K) = V_{dcerr}(K) - V_{dc}(k)$

When Vdcerr is sent to the DC link voltage controller, it lowers error, and its output—which is referred to as ωref—is provided as,

$\omega_{ref}(K) = \omega_{ref}(k-1) + K_{pdc} V_{dcerr}(k) = K_{idc}\{V_{dcerr}(K) - (k-1)\}$

Hence, in the DC link voltage controller, Kidc is the integral gain and Kpdc is the proportional gain.

At the kth sampling instant, the error between ωref and ωmest is as follows:

$\omega_{err}(k) = \omega_{ref}(K) - \omega_{mest}(k)$

The speed PI controller receives this mistake as input, and the result is provided as reference torque (Teref), which is defined as

$T_{eref}(k) = T_{eref}(k-1) + K_{p\omega}\omega_{err}(k) + K_{i\omega}\{\omega_{err}(k) - \omega_{err}(k-$

where Kiω, an integral gain, and Kpω, a proportional gain, are used in the speed controller.

Using the reference torque, one can compute the reference quadrature-axis current (iqref) as follows:

$$i_{qref} = \frac{2}{3 * p * \psi_m} * T_{eref}$$

The PMSM speed is restricted to its basic speed while using WPS. Thus, reference direct axis current (idref) is maintained at zero and field weakening is not required. Additionally, unity power factor functioning is guaranteed. In order to estimate the reference motor currents iaref, ibref, and icref, idref and iqref are converted from dq0 to abc. The hysteresis current controller, as shown in Fig. 8, is used to generate switching signals (SI1–SI6) by comparing these reference currents to detected stator currents and exploiting the error.

4. RESULTS AND DISCUSSION

A created laboratory prototype is used to verify the proposed system performance through experimentation. The created prototype consists of a solar PV array simulator (ETS600×17DPVF AMETEK make), a VSI (MD B6CI 600/415-35F SEMIKRON make), and a PMSM (TETRA 115SR5.2 MOTOR POWER COMPANY make), which are connected to a DC generator (BENLEC make). Because of the limitations in the laboratory, the water pump is the DC generator (DCG). A DC-DC buck converter is used to create a pump emulator, which realizes the pump's characteristics. The load characteristic of the pump is then obtained by controlling the buck converter's duty ratio, as seen in Figure 9. The digital signal processor (dSPACE-1202) provides the control signals. The Hall-Effect voltage and current sensor (LEM manufacture LA55P and LV25P, respectively) is used to sense the voltage and current. Signal isolation is accomplished by use of the opto-coupler (6N136). A DSO (Agilent, model number

7014A) is used to obtain the test results. Appendices include the comprehensive specifications for the characteristics and parts of the SWP system.

4.1 Development of Pump

Emulator An emulator for a pump is utilized in place of the real pump because of limitations in the laboratory. In the lab, a pump emulator is created to simulate the load profile of a real pump. Pump affinity law states that the following equation determines a water pump's load profile:

$$T_{eref} = K\omega^{2}_{rest}$$

For the pump emulator, Teref is regarded as the reference torque. After comparison, the estimated torque and the reference torque are supplied to the PI controller. The buck converter, which feeds the resistive load and determines the loading characteristics of the water pump, uses the output of the PI controller as the duty ratio.

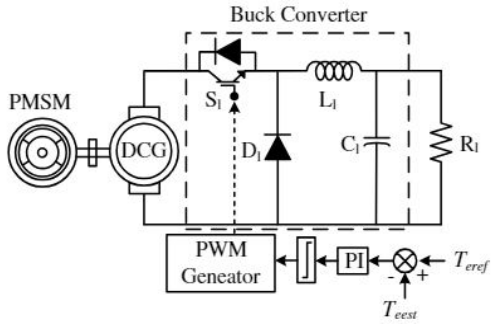

Fig. 9 Design and control of pump emulator

4.2 Starting and Steady State Responses

Following a thorough examination, the suggested WPS's initial and steady state behaviors are documented and given below. Figures 10(a–c) and 10(d–f) show The initial and steady state performance, respectively, at 1000 W/m2 and 500 W/m2 of solar insolation at a constant 250 C ambient temperature. The obtained results can be used to realize a soft beginning performance. Various PV array indices are recorded, and Fig. 10(a) shows that while the solar PV voltage initially stays at its open circuit voltage value, the suggested MPPT approach allows Vpv to decrease to its MPP value when the pump is turned on. The PV voltage and DC link voltage are the same because of the single stage architecture used. At MPP functioning, the PV current (Ipv) also rises from 0 to its steady state value of current. It can be observed that the reference speed (ωref) produced by the voltage controller is followed by the estimated speed of PMSM (ωmest). The fluctuation of PV array power (Ppv), estimated electromagnetic power (Peest), phase-specific stator current (ia), and estimated pump speed (ωmest) are displayed in Fig. 10(b). The Ppv climbs from zero as soon as the SWP system turns on and reaches the steady state value in around three seconds. When the motor is first gaining the first accretion, it pulls a lot of current. Ia also reaches and settles at its steady state value once the motor speed reaches it. Fig. 10 (c) displays the stator currents' steady state responses (ia, ib, and ic). It is apparent that sinusoidal stator currents are drawn by the PMSM. The suggested system exhibits a stable and robust reaction, even when exposed to 500 W/m2 of solar insolation. The voltage controller generates a lower reference speed based on the amount of solar electricity that is available. In practical terms, the anticipated speed follows the reference speed. 500 W/m2 of sinusoidal steady state current is drawn by the PMSM. a constant condition.

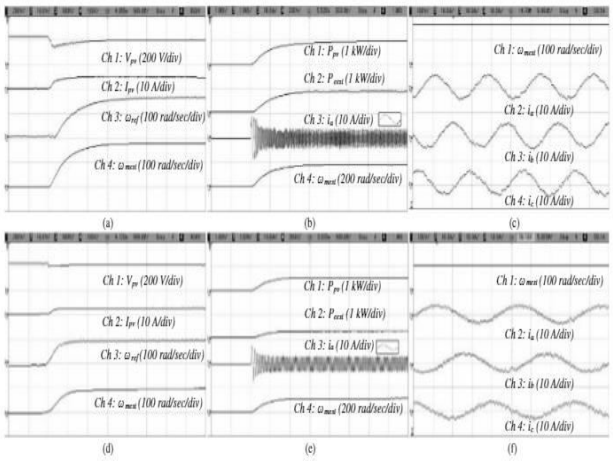

Fig. 10 Starting and steady state response of SWP system

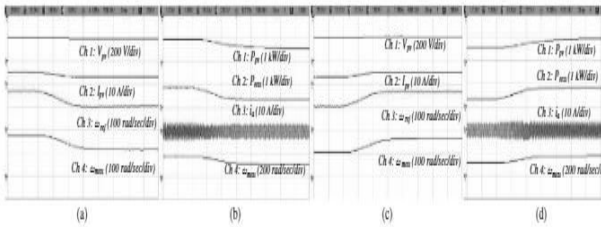

Fig. 11 Dynamic response of SWP system

A velocity of around 100 rad/sec is noted at lower solar insolation levels. The results of Figs. 10(d–f) indicate that the suggested system functions well even at 500 W/m2 of solar insolation.

4.3 Dynamic Response during Solar Insolation Change

By altering the solar insolation, the SWP system's dynamic behavior may be observed, as shown in Fig. 11. The behavior of the suggested WPS for variations in solar insolation from 1000 W/m2 to 500 W/m2 and returning to 1000 W/m2 is shown in Figs. 11 (a-b) and Figs. 11 (c-d), respectively. It is understood that the power production of the PV array is directly impacted by the decrease in insolation. When determining the PV array's peak power extraction, the Vpv settles at a new MPP value. When the insolation drops from 1000 W/m2 to 500 W/m2, the PV array current Ipv falls to about half of its previous value, which also causes the PV power Ppv to drop to about half of its prior value. As solar insolation decreases, the other system indices, including ωref, ωest, Ppv, Peest, and Ia, follow the trend and stabilize at a lower steady state value. The SWP system functions in the opposite way to bring solar insolation back to 1000 W/m2.

4.4 MPPT Performance

Using the single sensor based MPPT approach, the MPPT behavior of the SWP system is displayed in Figs. 12(a-b) at 500 W/m2 and 1000 W/m2 of solar insolation, respectively. At both solar insolations, an exceptional MPPT with a tracking efficiency exceeding 99% is found.

4.5 Performance of the Flux Estimator

For the purpose of estimating stator flux, the system under presentation suggests a flux estimator based on MMGI. Fig. 13 depicts the suggested flux estimator's steady state behavior. Figure 13 makes it abundantly evident that the predicted stator fluxes (ψα and ψβ) are sinusoidal in nature because of the usage of an MMGI based structure that has the capacity to reject dominating lower harmonics in addition to removing DC offset. Since the fluxes are sinusoidal, there are no ripples in the estimated speed (ωmest). Furthermore, the effective tracking of the rotor position (θeest) is also seen.

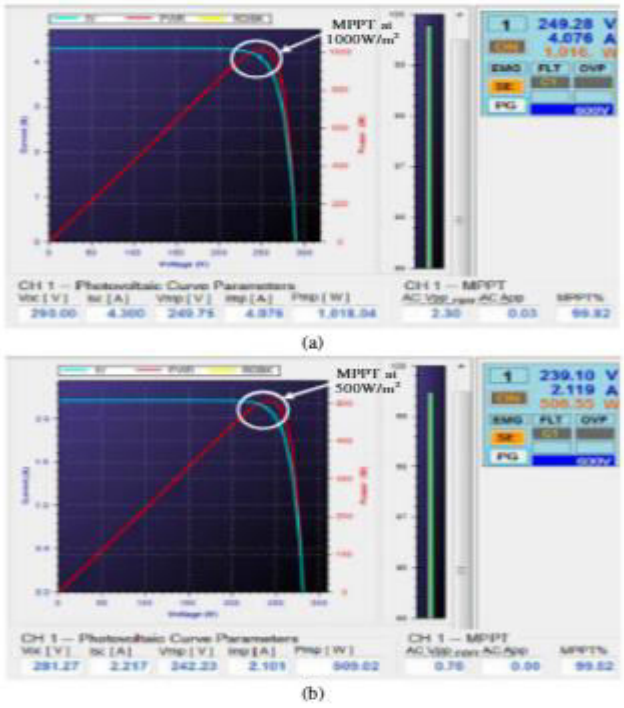

(a)

(b)

Fig. 12 MPPT Performance

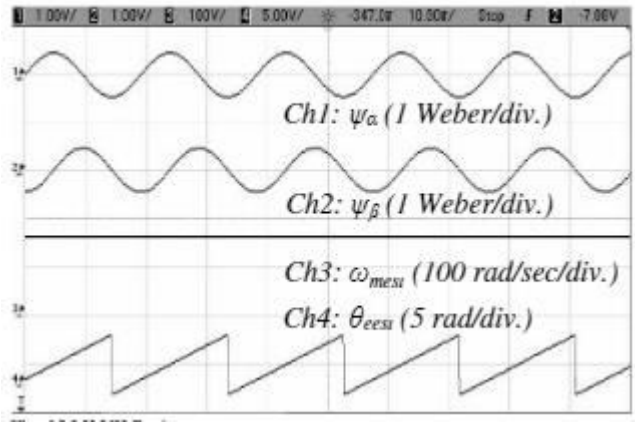

Fig. 13 MMGI Performance

5. CONCLUSION

A laboratory prototype of a reduced sensor-based SWP system is constructed and tested under various operating situations to verify its viability. For stator flux estimation, a mixed multi-resonant generalized integrator has been developed. Comparative frequency domain study has shown that, when compared to standard SOGI, the suggested structure has offered superior harmonics reduction and DC offset rejection capacity. The lower order harmonics have been successfully reduced by the multi-resonant structure. The SWP system functions well in a range of solar insolation scenarios, and the suggested single sensor MPPT algorithm has produced an excellent MPPT capability that has successfully extracted the maximum power from the PV array without degrading system performance. A picture of the SWP system running smoothly is displayed. System costs have decreased as a result of the fewer sensors. By reducing the losses experienced in the intermediate stage converter, the single stage architecture has improved system efficiency. Thus, it can be concluded that this WPS provides a workable option for a dependable solar water pumping system because of its advantages of a straightforward, compact design, effective operation, and low cost.

REFERENCES

[1] PTI, “MPUVN rooftop solar gets lowest ever tariff of Rs 1.38 per unit,” The Economic Times, Oct. 05, 2018. [Online]. Available: -lowest-ever-tariff-of-rs-1-38-per-unit/66087009 [Accessed Dec. 24, 2018].

[2] M. Rezkallah, A. Chandra, M. Tremblay and H. Ibrahim, “Experimental Implementation of an APC With Enhanced MPPT for Standalone Solar Photovoltaic Based Water Pumping Station,” IEEE Trans. Sust. Energy, vol. 10, no. 1, pp. 181-191, Jan. 2019.

[3] M. A. Elgendy, B. Zahawi and D. J. Atkinson, “Comparison of Directly Connected and Constant Voltage Controlled Photovoltaic Pumping Systems,” IEEE Trans. Sust. Energy, vol. 1, no. 3, pp. 184-192, Oct. 2010.

[4] B. Subudhi and R. Pradhan, “A Comparative Study on Maximum Power Point Tracking Techniques for Photovoltaic Power Systems,” IEEE Trans. Sust. Energy, vol. 4, no. 1, pp. 89-98, Jan. 2013.

[5] S. Saravanan and N. R. Babu, “Maximum power point tracking algorithms for photovoltaic system – A review,” Renew. and Sust. Energy Reviews, vol. 57, pp. 192-204, 2016.

[6] M. Killi and S. Samanta, “An Adaptive Voltage-Sensor-Based MPPT for Photovoltaic Systems With SEPIC Converter Including Steady-State and Drift Analysis,” IEEE Trans. Ind. Elect., vol. 62, no. 12, pp. 7609-7619, Dec. 2015.

[7] S. Jain, R. Karampuri and V. T. Somasekhar, “An Integrated Control Algorithm for a Single-Stage PV Pumping System Using an Open-End Winding Induction Motor,” IEEE Trans. Ind. Elect., vol. 63, no. 2, pp. 956-965, Feb. 2016.

[8] M. A. Elgendy, B. Zahawi and D. J. Atkinson, “Assessment of Perturb and Observe MPPT Algorithm Implementation Techniques for PV Pumping Applications,” IEEE Trans. Sust. Energy, vol. 3, no. 1, pp. 21- 33, Jan. 2012.

[9] A. K. Mishra and B. Singh, “Design of solar-powered agriculture pump using new configuration of dual-output buck–boost converter,” IET Renew. Pow. Gen., vol. 12, no. 14, pp. 1640-1650, Oct. 2018.

[10] M. A. Elgendy, B. Zahawi and D. J. Atkinson, “Assessment of the Incremental

Conductance Maximum Power Point Tracking Algorithm," IEEE Trans. Sust. Energy, vol. 4, no. 1, pp. 108-117, Jan. 2013.

[11] R. Kumar and B. Singh, "Single Stage Solar PV Fed Brushless DC Motor Driven Water Pump," IEEE J. Emerging Selected Topics Pow. Elect., vol. 5, no. 3, pp. 1377-1385, Sept. 2017.

[12] S. Murshid and B. Singh, "Simulation and hardware implementation of PMSM driven solar water pumping system," in proc. IEEE Int. Conf. Pow., Inst., Ctrl and Comp. (PICC), Thrissur, pp. 1-6, 2018.

[13] F. Karbakhsh, M. Amiri and H. Abootorabi Zarchi, "Two-switch flyback inverter employing a current sensorless MPPT and scalar control for low cost solar powered pumps," IET Renew. Pow. Gen., vol. 11, no. 5, pp. 669-677, 2017.

[14] C. Urayai and G. A. J. Amaratunga, "Single-sensor maximum power point tracking algorithms," IET Renew. Pow. Gen., vol. 7, no. 1, pp. 82-88, Feb. 2013.

[15] A. Pandey, N. Dasgupta and A. K. Mukerjee, "A Simple Single-Sensor MPPT Solution," IEEE Trans. Pow. Elect., vol. 22, no. 2, pp. 698-700, March 2007.